

Computational Analysis of Aluminum Corrosion Inhibition Potentials Using Selected Thiosemicarbazide Derivatives

ABSTRACT

Aluminum, a metal with a rich cultural history, remains vital in numerous industrial applications. However, its susceptibility to corrosion in harsh environments poses significant challenges. Traditional corrosion inhibitors have been developed to counteract this issue, but they often come with drawbacks such as high costs and harmful environmental and health impacts. This study employed density functional theory (DFT) to evaluate the potential of two compounds—2-(4-methylbenzylidene)hydrazinecarbothioamide (MBHC) and N-phenylhydrazinecarbothioamide (PHC)—as corrosion inhibitors for aluminum surfaces. Electrostatic potential (ESP) analysis revealed that the sulphur and nitrogen atoms in these compounds exhibit nucleophilic behaviour, making them effective for corrosion inhibition. The research highlighted MBHC's superior performance over PHC in corrosion prevention. Molecular orbital theory and Monte Carlo simulations demonstrated that MBHC formed stronger and more stable complexes with the aluminum surface, as reflected in its higher adsorption energy of -461.73 eV compared to PHC's -163.43 eV. These findings pave the way for developing environmentally friendly inhibitors to protect aluminum surfaces, combining efficiency with sustainability.

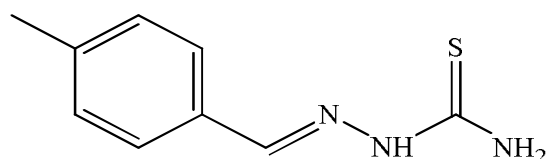
Keywords: adsorption energy; DFT; Potentials; Aluminum; inhibitor; Simulation

1. INTRODUCTION

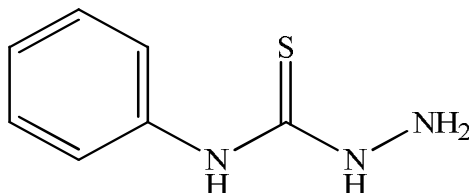
In the crust of the globe, aluminum is the third most frequent metal overall and the fourth most prevalent in the crust specifically. After iron, aluminum is typically regarded as the second most significant metal. It has unique mechanical characteristics because of its low density (2.7 g cm^{-3}), which is just about one-third that of mild steel. As a result, aluminum and its alloys offer a high strength-to-weight ratio. In addition, a wide range of metal machining processes can be readily applied to them, and they exhibit good electrical and thermal conductivity. Furthermore, aluminum and its alloys have been fully recycled and reused, meaning that the items made from recycled metal are similar to those that were made before recycling in terms of quality and attributes (Olufumilayo & Olakunle, 2021). Because of its excellent strength-to-weight ratio and affordable price, aluminum and its alloys are widely used in aerospace, automotive, electrical parts, building, packaging, and chemical industries (Rouniya & Shandilya, 2019; Becker, 2019; Emadi et al., 2019). In non-aggressive conditions, an Al_2O_3 coating naturally forms on the alloy surface to preserve aluminum (Arrousse et al., 2022). Because of its numerous flaws and pores, the oxide layer is rapidly dissolved by corrosive OH^- or Cl^- ions. However, because key alloy components like copper and magnesium are present, aluminum and its alloys are highly susceptible to localized corrosion in harsh conditions. This alloy's microstructure is rather complicated, and several phases with different compositions have been found (Liu et al., 2017). Since an

36 oxide layer forms on aluminum and prevents the metal from oxidizing further, aluminum has
37 a high level of corrosion resistance in both aqueous solutions and the environment.
38 However, in some conditions, such as acidic media, aluminum becomes extremely prone to
39 corrosion. There are already several efficient protection techniques available, including
40 surface coatings, organic inhibitor addition, anodic oxidation protection, and plasma
41 electrolytic oxidation protection (Gummanar et al., 2023; Markus, 2019; Yang et al., 2017).
42 Inhibitors, which prevent corrosion on metal surfaces by forming a protective coating on
43 them, are the most widely used and least expensive of them across a variety of industries.
44 Products with an organic base are frequently used to prevent corrosion. Organic compounds
45 with heteroatoms (N, S, and O) in a conjugated system exhibit excellent efficacy in
46 preventing metal corrosion (Verma et al., 2016; Iroha & Akaranta, 2020; Nkem et al., 2021).
47 The effectiveness of corrosion inhibition has been precisely established by experimental
48 research, however, the precise mechanism by which inhibitors contribute most to corrosion
49 inhibition has not been thoroughly addressed. Costs and time for research are significant.
50 These issues are bridged by the theoretical study, which is now backed by sufficient
51 hardware and software. The electron density of the molecule determines the corrosion
52 inhibition efficiency, and theoretical research can determine this density with high accuracy.
53 When evaluating corrosion inhibition in a molecule, theoretical research is just as important
54 as actual research. Questions concerning experimental results based on the interactions of
55 organic inhibitors with metal surfaces can be addressed using quantum chemical
56 computations (Ebenso et al., 2021). Verma et al. (Verma et al., 2021) underlined in their
57 thorough review the application of quantum chemistry techniques to corrosion inhibitor
58 investigations of several organic compounds. Uzah, (2024) theoretically explored the
59 interactions between selected thiosemicarbazide derivatives on Al (111) and Cu (111)
60 surfaces by using the B3LYP/6-311G (d, p) method. The Electrostatic potential (ESP)
61 surface analysis used to identify the reactive areas., was considered, and Fukui indices were
62 determined for N+1 and N-1 electron species, at the geometry of the selected
63 thiosemicarbazide derivatives reference N-electron. Their results showed that the ΔE , E_{LUMO} ,
64 χ , η , E_{HOMO} , σ , and ΔN localization and the condensed Fukui functions (f- and f+) analysis in
65 the reactive region were instrumental in characterizing organic adsorbates.
66 Ibrahim et al. (2023) investigated the potentiality of the 6-mercaptopurine (MP) and 6-
67 thioguanine (TG) expired drugs toward the corrosion inhibition of the aluminum (Al) (111)
68 surface, using the B3LYP/6-311G basis set. ΔE , E_{HOMO} , E_{LUMO} , μ , and η parameters were all
69 calculated for each of the expired drugs, both in the liquid and gas phases, of which results
70 show no significant difference in the structures of the expired drugs. Khabazi and
71 Chermahini, (2023) presented Two different isomeric forms of tetrazole molecules and their
72 derivatives, including 1H and 2H tautomers, as corrosion inhibitors were studied in two
73 configurations, parallel and perpendicular to the Cu (1 1 1) surface, using the 6-31GDFT
74 method. The Mulliken partial charges, E_{HOMO} , E_{LUMO} , ΔE , total hardness (η), electronegativity
75 (χ), and electron fraction transitions from the anti-corrosion molecule to the copper atom
76 (ΔN), were, calculated, and the IE was associated with ΔE and the frontier orbital electron
77 density. It was observed that tetrazole molecules were physically adsorbed onto the copper
78 surface.
79 The performance of each inhibitor concerning its structure and orientation, as well as the
80 mechanism by which an inhibitor clings to metal surfaces, may be fully explained by the use
81 of the methods of density functional theory and Monte Carlo simulation (Sulaiman et al.,
82 2019). Hadisaputra et al., (2022) investigated the real environment conditions of corrosion
83 inhibition in the solution phase can be replicated by the Monte Carlo simulation. The
84 corrosion inhibition efficiency of phthalimide derivatives was PP-OCH3 > PP-CH3 > PP-H >
85 PP-Cl > PP-NO2. The theoretical study was consistent with previously reported experimental
86 results. The surface interactions between the inhibitor molecules and the metal surface
87 were investigated by Oukhrib et al., (2021) using molecular dynamics simulations and Monte
88 Carlo (MC) simulations. As a result, they found that the inhibitor pyrazolynucleosides have

89 strong interactions with Cu (111) surface, and therefore have excellent predictive inhibition
 90 power against copper corrosion. Derivatives of thiosemicarbazide are widely used in medical
 91 chemistry to create medications that combat germs, fungi, viruses, depression, etc. Its
 92 primary biological functions are DNA doping transporter, anticancer, and DNA retaining
 93 capacity. No computational study has been published on the corrosion prevention of MBHC
 94 and PHC derivatives of Thiosemicarbazide on Aluminium Surfaces. However, some of these
 95 derivatives are said to be effective deterioration inhibitors for Aluminium in acidic media. The
 96 corrosion inhibition of MBHC and PHC (Fig.1): on Al (111) surfaces are studied in this work,
 97 along with the impacts of quantum parameters and the molecule's adsorption process.



98 *(E)*-2-(4-methylbenzylidene)hydrazinecarbothioamide (MBHC)



99 *N*-phenylhydrazinecarbothioamide (PHC)

100 **Fig.1. The chemical structures of MBHC and PHC**

101
 102 **2. COMPUTATIONAL DETAILS**

103
 104 **2.1 DFT Study**

105
 106 Studies on corrosion inhibition commonly employ the density functional theory (DFT). When
 107 it comes to organic compounds' ability to suppress corrosion, the DFT approach provides an
 108 accurate description. Predicting the chemical properties of chemical species, such as the
 109 maximum occupied molecular orbital–lowest unoccupied molecular orbital (HOMO–LUMO),
 110 electron affinity (A), ionization potential (I), energy gap (ΔE), hardness (η), fraction of
 111 electrons transferred (ΔN), softness (σ), and electronegativity (χ), is the main goal of
 112 research on inhibitors. The following paper used theoretical calculations to anticipate the
 113 effectiveness of the Thiosemicarbazide derivatives *E*-2-(4-
 114 methylbenzylidene)hydrazinecarbothioamide (MBHC) and *N*-
 115 phenylhydrazinecarbothioamide (PHC) (Fig.1). Employing the Gaussian 09W programming
 116 suite, the B3LYP technique coupled to 6-311G+ (d,p) basis sets were utilized to optimize all
 117 compounds geometrically. This approach is widely used in the research of organic corrosion
 118 inhibitors. Then, several relevant global and local variables of the molecule's electronic
 119 configuration were computed. The I, A, ΔE , ΔN , η , σ , χ , E_{LUMO} , and E_{HOMO} as well as maps of
 120 electrostatic potential were also computed (Verma et al., 2021; Khabazi&Chermahini,2023).

121
$$A = E_{LUMO} \quad (1)$$

122
$$I = E_{HOMO} \quad (2)$$

123
$$\Delta E = E_{LUMO} - E_{HOMO} \quad (3)$$

124
$$\eta = \left(\frac{\delta^2 E}{\delta N^2}\right)_v = \left(\frac{\delta \mu}{\delta N}\right)_v = \frac{E_{LUMO} - E_{HOMO}}{2} \quad (4)$$

125
$$\sigma = 2 \left(\frac{\delta N}{\delta \mu} \right)_{v(r)} = \frac{1}{\eta} = \frac{2}{\Delta E E_{LUMO} - E_{HOMO}} \quad (5)$$

126
$$\chi = \frac{-(E_{HOMO} + E_{LUMO})}{2} \quad (6)$$

127
$$\Delta N = \frac{(\chi_{Al} - \chi_{inh})}{2 \times (\eta_{Al} - \eta_{inh})} \quad (7)$$

128 Where, $\chi_{Al} = 4.26$ eV and χ_{inh} = absolute electronegativities of the aluminum and inhibitor
 129 respectively. $\eta_{Al} = 0$ eV and η_{inh} = absolute hardness of the aluminum and inhibitor
 130 respectively.

131 **2.2 Monte Carlo simulation.**

132

133 The interactions between the chemical compounds and metal surface were theoretically
 134 studied by the Monte Carlo simulation The simulation was conducted in Material Studio 2020
 135 (Biovia, USA) using COMPASS force-field (condensed phase), on the Al (111) surface (three
 136 dimensions to the slab model) under periodic boundary conditions. The energies and
 137 chemical adsorption mechanisms components were calculated using the Ewald and atom-
 138 based summations, or responsibly to the Adsorption Locator module, built-in Materials
 139 Studio 2020 which used Monte Carlo simulations to pinpoint the most stable arrangement of
 140 the adsorbates on the Al (111) surface is the most stable of the many aluminum surfaces
 141 (Bourzi et al., 2020; Uzah, & Mbonu, 2023),

142

143 **3. RESULTS AND DISCUSSION**

144

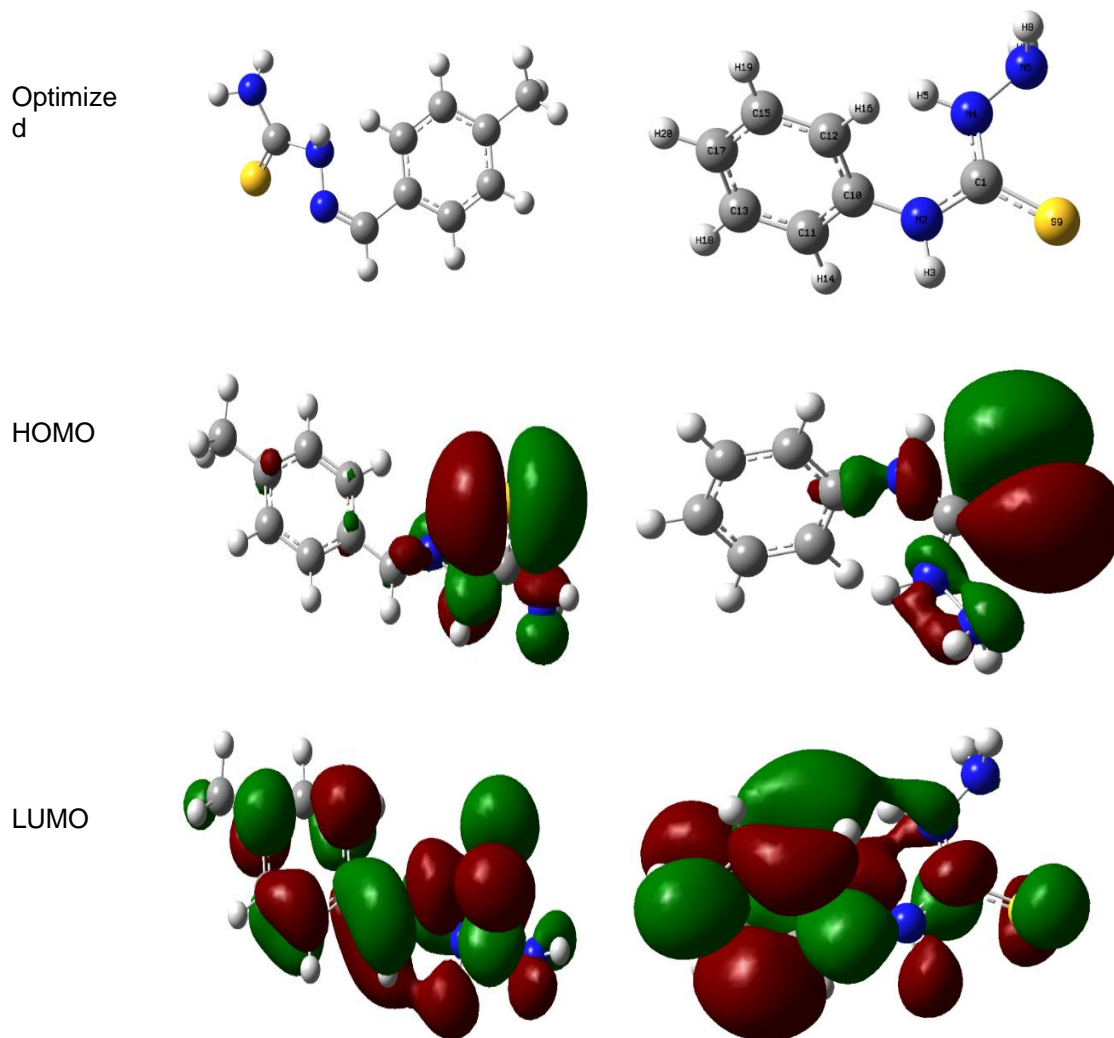
145 **3.1. DFT Results**

146

147 Table 1 is a list of the calculated quantum chemical parameters. Given structures that are
 148 optimized HOMO and LUMO density distribution of PHC and MBHC, Fig.2 shows that PHC
 149 has fewer adsorption centers than MBHC, indicating that MBHC has a higher capacity for
 150 high-protective adsorption. As a result, the high E_{HOMO} energy increases the inhibition
 151 performance by reflecting a greater connection between the molecule and the metal surface
 152 through the donor-acceptor process. (Guo et al., 2017; Hadisaputra et al., 2022). MBHC can
 153 readily interchange electrons with the iron surface, as evidenced by its higher E_{HOMO} value of
 154 -0.218 eV compared to PHC's -0.210 eV. On the other hand, the fact that MBHC has a
 155 lower E_{LUMO} value indicates that it is an excellent inhibitor of electron acceptance and
 156 supports its superior performance (-0.018 eV) over PHC (-0.042 eV)
 157 (Khabazi&Chermahini,2023; Uzah& Mbonu, 2024). Better adsorption on aluminum surfaces
 158 is indicated by the narrower energy gap (ΔE) of MBHC (0.1493 eV) (Fouda et al., 2023).
 159 Further quantum chemical characteristics were derived, including ionization potential ($I =$
 160 $-E_{HOMO}$), electron affinity ($A = -E_{LUMO}$), global softness (σ), global hardness (η),
 161 electronegativity (χ), and number of electron transfer (ΔN). The literature claims that a
 162 molecule with a high (η) value is less reactive, whereas a high (χ) value indicates that the
 163 molecule may find it difficult to transfer its electrons to an acceptor (Kaya & Kaya, 2015;
 164 Uzah et al., 2023). The findings in Table 1 demonstrate that MBHC has lower (η) and (χ)
 165 values than PHC, indicating that it is more reactive and can transfer electrons through donor-
 166 acceptor interactions with metal molecules. (Uzah,2024). Within a group of inhibitors, the
 167 electron donation tendency is described by the charge transfer rate ΔN . According to
 168 Lukovits ((Jabri et al., 2022; Uzah et al., 2023), the efficiency of the inhibition increases as
 169 the electron donor capacity at the steel/electrolyte increases if $\Delta N < 3.6$. Table 1 displayed
 170 ΔN values are all 3.6 lower than the original values. Therefore, the quantum chemical
 171 characteristics of MBHC performed better at its level of inhibition than the PHC inhibitor.

172

Inhibitor	MBHC	PHC
-----------	------	-----



173 Fig.2. The frontier molecular orbital density distribution for MBHC and PHC
174 investigated compounds (Optimized, HOMO, and LUMO).
175

176

177

178

179 Table 1. The quantum chemical variables for MBHC and PHC inhibitors using
the B3LYP/6-31G+ (d, p) basis set.

C	E_{LUMO}	E_{HOMO}	ΔE	H	Σ	X	ΔN_{AI}
MBHC	-0.0180	-0.2178	0.1493	0.0747	13.40	0.143	-20.66
PHC	-0.0422	-0.2095	0.1673	0.0837	11.95	0.0948	-18.54

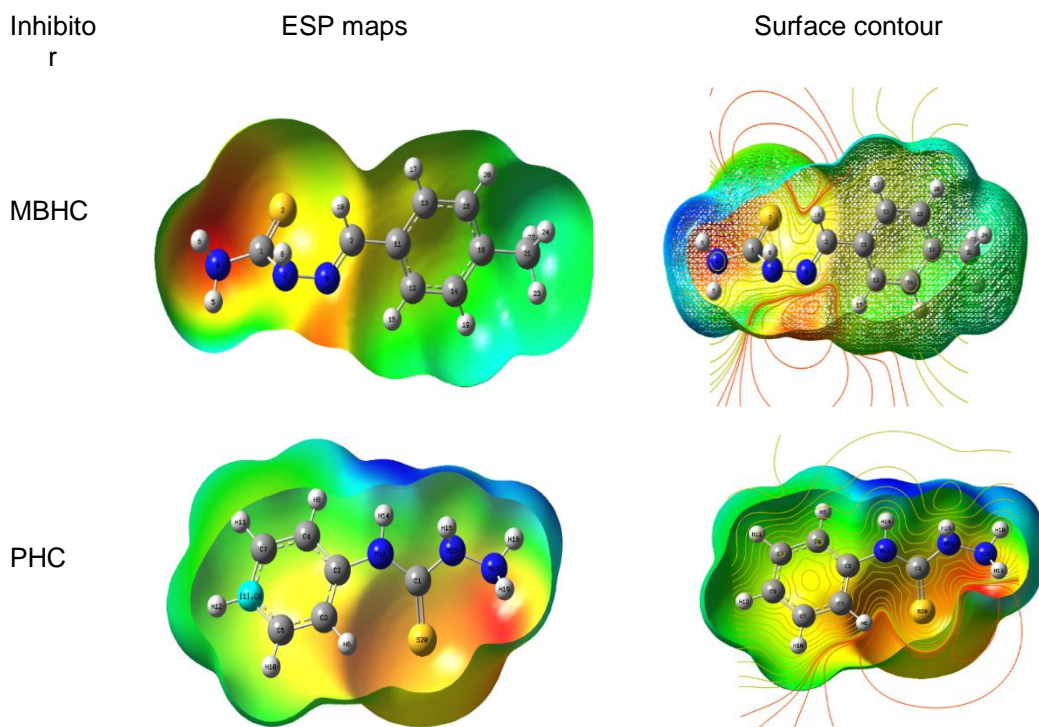
180

181 3.2 Electrostatic Potential (ESP) Map

182

183 ESP map displays the three-dimensional charge distribution of the molecule (Fig.3). This
184 map aids in the visualization of the molecule's variable charge areas, which helps forecast
185 electrophilic and nucleophilic molecule-attack scenarios (Thakur & Kumar, 2023). The

186 highest positive region vulnerable to nucleophile assault is shown as blue in the ESP plot.
187 On the other hand, the negative region that is vulnerable to electrophilic attack is shown in
188 red. The MBHC and PHC sulfur and nitrogen atoms are found to have the highest electron
189 density. Consequently, it is expected that these atoms will actively participate in the
190 adsorption process on the Aluminum surface.
191
192
193



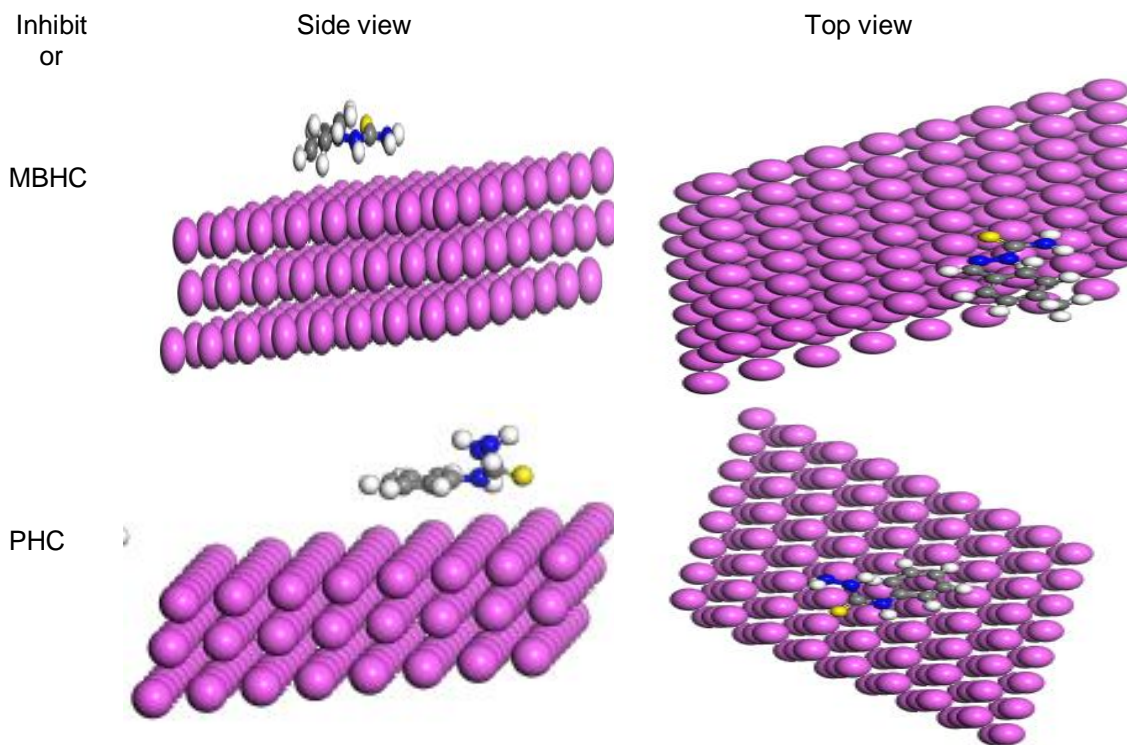
194 **Fig.3. ESP maps and surface contours illustration of the MBHC and PHC**
195 **investigated**

196 197 **3.3 Monte Carlo simulation.** 198

199 To reduce the amount of contact area between the metal surface and corrosion-causing
200 materials (such as water, acidic, or alkaline media), molecules need to align their structures
201 as closely as possible in parallel to the metal surface. Adsorption is the term for this process.
202 Therefore, Monte Carlo simulation was applied to determine and identify the inhibitors under
203 evaluation and their ability to adsorb onto the surface of Al (111). Fig.4 shows the optimal
204 MBHC and PHC adsorption mode on the aluminum surface under study.

205 Table 2 displays the molecule under investigation's adsorption characteristics, which include
206 total energy, rigid adsorption energy, adsorption energy, and deformation energy. We have
207 previously defined these parameters (Bourzi et al., 2020; Uzah, 2025). in our previous work.
208 The total rigid adsorption energy before and after an adsorbate's surface relaxation is known
209 as the "adsorption energy," and it is the most significant energy characteristic in adsorption.
210 Table 2 indicates that the inhibitor attaches to the surface of Al (111) spontaneously based
211 on the negative value of the adsorption energies (Uzah, & Mbonu, 2023). The differential

212 adsorption energy (dE_{ad}/dN_i), which is the energy needed or released to remove a portion of
 213 the adsorbate (i.e., desorption energy), is defined by assuming that the surface energy of Al
 214 is zero. The inhibitor's adsorption energy of $-461.73 \text{ kcal mol}^{-1}$ for MBHC and $163.43 \text{ kcal mol}^{-1}$
 215 mol^{-1} for PHC and its desorption energy of $--461.73 \text{ kcal mol}^{-1}$ (MBHC) and -80.754 kcal
 216 mol^{-1} (PHC) indicate that the adsorption process is substantially preferred. The inhibitor
 217 preferentially adsorbs on the Al (111) surface with little to no competition because it adsorbs
 218 with significantly less energy, even in the presence of water ($--4.28 \text{ kcal mol}^{-1}$) (Benzidia et
 219 al., 2022; Uzah, 2025).
 220
 221



222
 223 **Fig.4. The most appropriate conformation for adsorption of the MBHC and PHC**
 224 **molecules on Al (111)**
 225
 226
 227
 228

229 **Table 2. Results and descriptors measured by the Monte Carlo simulation for**
 230 **adsorption of MBHC and PHC molecules on Al (111)**
 231

Compound	dE_{ad}/dN_i	Adsorption energy	Rigid adsorption energy	Deformation energy	Total energy
MBHC	-461.73	-461.73	-30.707	-431.02	-3.272
PHC	-80.75	-163.43	-55.83	-107.61	-5.75
Water	-4.281	-8.297	-7.346	-0.950	-7.346

232

233 **4. CONCLUSION**

234

235 The corrosion inhibition potential of E)-2-(4-methylbenzylidene)hydrazinecarbothioamide
236 (MBHC) and N-phenylhydeazinecarbothioamide (PHC) was analyzed and measured using
237 density functional theory calculations employing the B3LYP/6-31G+ (d,p) basis set. This was
238 done to determine whether these compounds had a potentially strong ability to inhibit
239 corrosion in aluminum and its alloys. In contrast to PHC, MBHC has a lower electronegativity
240 and ΔE , (0.1612 eV) values, which may be attributed to the presence of an aromatic ring and
241 heteroatom in its structure, which demonstrated a stronger and mutual connection between
242 the inhibitor and the metallic surface according to the results of the Density Functional
243 Theory analysis: Furthermore, the results showed that MBHC had the largest ΔN value
244 (0.258232 eV), indicating improved chemical stability and reactivity. In light of this, MBHC is
245 more likely than PHC to react as an electron donor, which effectively inhibits the
246 corrosion of alloys including aluminum. MBHC was predicted by Monte Carlo simulations to
247 function as a more potent anti-corrosion agent than PHC, particularly in acidic environments.
248

249

DISCLAIMER (ARTIFICIAL INTELLIGENCE)

250 Authors hereby declare that NO generative AI technologies such as Large Language Models
251 (ChatGPT, COPILOT, etc.) and text-to-image generators have been used during the writing
252 or editing of this manuscript.

253 **ACKNOWLEDGEMENTS**

254

255 The authors would like to acknowledge the Federal University of Petroleum Resources,
256 Effurun for creating an enabling environment for this research work.

257

258

259

COMPETING INTERESTS

260 **Competing interests** The authors declare no conflict of interest.

261

262 **AUTHORS' CONTRIBUTIONS**

263

264 The manuscript was written with contributions from all authors. All authors read and approved
265 the final manuscript

266

267

268

REFERENCES

269

270

271

272

273

274

275

276

277

278

1. Arrousse, N., Fernine, Y., Al-Zaqri, N., Boshala, A., Ech-chihbi, E., Salim, R., El Hajjaji, F., Alami, A., EbnTouhamie, M., Taleb, M. (2022). Thiophene derivatives as corrosion inhibitors for 2024-T3 aluminum alloy in hydrochloric acid medium. *RSC Advances*, 12, 10321. DOI: 10.1039/d2ra00185c
2. Becker, M. (2019). Chromate-free chemical conversion coatings for aluminum alloys, *Corrosion Review*, 37, 321–342. <https://doi.org/10.1515/correv-2019-0032>
3. Benzidia, B., Barbouchi, M., Hsissou, R., Zouarhi, M., Erramli, H., Hajjaji, N. (2022). A combined experimental and theoretical study of green corrosion inhibition of bronze B66 in 3% NaCl solution by Aloe saponaria (syn. Aloe maculata) tannin extract. *Current Research in Green and Sustainable Chemistry*, 5, 100299. <https://doi.org/10.1016/j.crgsc.2022.100299>

- 279
280
281
282
283
284
285
286
287
288
289
290
291
292
293
4. Bourzi, H., Oukhrib, R., El Ibrahim, B., Oualid, H. A., Abdellaoui, Y., Balkard, B., El Issami, S., Hilali, M., Bazzi, L., Len, C. (2020). Furfural analogs as sustainable corrosion inhibitors—predictive efficiency using DFT and Monte Carlo simulations on the Cu (111), Fe (110), Al (111) and Sn (111) surfaces in acid media. *Sustainability*, 12, 3304; doi:10.3390/su12083304
 5. Ebenso, E. E., Verma, C., Olasunkanmi, L. O., Akpan, E. D., Verma, D. K., Lgaz, H., Quraishi, M. A. (2021). Molecular modeling of compounds used for corrosion inhibition studies: a review. *Physical Chemistry Chemical Physics*, 23, 19987–20027. <https://doi.org/10.1039/D1CP00244>
 6. Emadi, M., Beheshti, H., Heidari-Rarani, M., Aboutalebi, F. H. (2019). Experimental study of collapse mode and crashworthiness response of tempered and annealed aluminum tubes under axial compression, *Journal of Mechanical Science and Technology*, 33, 2067–2074. <http://dx.doi.org/10.1007/s12206-019-0410-2>
 7. Fouda, A. S., Etaiw, S. H. E, Ibrahim, A. M., El-Hossianya, A. A. (2023). Insights into using two novel supramolecular compounds as corrosion inhibitors for stainless steel in a chloride environment: experimental and theoretical investigation. *RSC Advance*, 13, 35305–35320. <https://doi.org/10.1039/d3ra07397a>
 8. Gummanar, N., Mokshanatha, P. B., Dyapur, P., Yallappa, G. N. (2023). Organic corrosion inhibitors for aluminum-based alloys –A Review. *Letters in Applied NanoBioScience*, 12, 4, 170. <https://doi.org/10.33263/LIANBS124.170>
 9. Guo, L., Obot, I. B., Zheng, X., Shen, X., Qiang, Y., Kaya, S., Kaya, C. (2017). Theoretical insight into an empirical rule about organic corrosion inhibitors containing nitrogen, oxygen, and sulfur atoms, *Applied Surface Science*, 406, 301–306. <http://dx.doi.org/10.1016/j.apsusc.2017.02.134>
 10. Hadisaputra, S., Purwoko, A. A., Hakim, A., Prasetyo, N., Hamdiani, S. (2022). Corrosion inhibition properties of phenyl phthalimide derivatives against carbon steel in the acidic medium: DFT, MP2, and Monte Carlo simulation studies. *ACS Omega*, 7, 33054–33066. <https://doi.org/10.1021/acsomega.2c03091>
 11. Ibrahim, M.A.A., Moussa, N.A.M., Mahmoud, A.H.M., Sayed, S.R.M., Sidhom, P.A., Abd El-Rahman, M.K., Shoeib T., Mohamed, L.A., (2023). Density functional theory study of the corrosion inhibition performance of 6-mercaptopurine and 6-thioguanine expired drugs toward the aluminium (111) surface. *RSC Advances*, 13, 29023–29034. <https://doi.org/10.1039/d3ra04954j>
 12. Iroha, N. B., Akaranta, O. (2020). Experimental and surface morphological study of corrosion inhibition of N80 carbon steel in HCl stimulated acidizing solution using gum exudate from Terminalia Mentaly. *SN Applied Sciences*, 2, 1514, <https://doi.org/10.1007/s42452-020-03296-8>.
 13. Jabri, Z., El Ibrahim, B., Jarmoni, K., Sabir, S., Misbahi, K., Rodi, Y. K., Mashrai, A., Hökelek, T., Mague, J. T., Sebbar, N. K., Essassi, E. (2022). New imidazo[4,5-b] pyridine derivatives: synthesis, crystal structures, Hirschfeld surface analysis, DFT computations, and Monte Carlo simulations. *Journal of Chemical Technology and Metallurgy*, 57(3), 451- 463. <https://doi.org/10.2174/0929867330666230426111650>
 14. Kaya, S., Kaya, C. (2015). A new method for calculation of molecular hardness: A theoretical study, *Computational and theoretical chemistry*, 1060, 66. <https://doi.org/10.1016/j.comptc.2015.03.004>
 15. Khabazi, M. E., Chermahini, A. N. (2023). DFT study on corrosion inhibition by tetrazole derivatives: investigation of the substitution effect. *ACS Omega*, 8, 9978–9994. <https://doi.org/10.1021/acsomega.2c07185>
 16. Liu, Y., Li, X. L., Jin, J. F., Liu, J. A., Yan, Y. Y., Han, Z. W., Ren, L. Q. (2017). Anti-icing property of bioinspired microstructure superhydrophobic surfaces and heat transfer model, *Applied Surface Science*, 400, 498–505. <https://doi.org/10.1016/j.apsusc.2016.12.219>
 17. Markus, B. (2019). Chromate-free chemical conversion coatings for aluminum alloys. *Corrosion Review*, 37, 32-39, <https://doi.org/10.1515/corrrev-2019-0032>.
- 294
295
296
297
298
299
300
301
302
303
304
305
306
307
308
309
310
311
312
313
314
315
316
317
318
319
320
321
322
323
324
325
326
327
328
329

- 330 18. Nkem, B., Iroha, N. B., Maduelosi, N. J. (2021). Corrosion inhibitive action and adsorption
331 behavior of *justicia secunda* leaves extract as an eco-friendly inhibitor for aluminum in acidic
332 media. *Biointerface Research in Applied Science*. 11 (5), 13019 – 13030.
333 <https://doi.org/10.33263/BRIAC115.1301913030>
- 334 19. Olufumilayo, O. J., Olakunle, O. J. (2021). Corrosion inhibition of Aluminum alloy by chemical
335 inhibitors: An overview. *IOP Conference Series: Material Science and Engineering*, 1107,
336 012170. <https://doi.org/10.1088/1757-899X/1/012170>.
- 337 20. Oukhrib, R., Abdellaoui, Y., Berisha, A., Oualid, H.A., Halili, J., Jusufi, K., El Had, M.A., Bourzi,
338 H., El Issami, S., Asmary, F.A., Parmar, V.S., Len, C. (2021) DFT, Monte Carlo and molecular
339 dynamics simulations for the prediction of corrosion inhibition efficiency of novel
340 pyrazolylnucleosides on Cu(111) surface in acidic media. *Scientific Reports*, 11, 3771.
341 <https://doi.org/10.1038/s41598-021-82927-5>.
- 342 21. Rouniya, A. K., Shandilya, P. (2019). Fabrication and experimental investigation of magnetic
343 field assisted powder mixed electrical discharge machining on machining of aluminum 6061
344 alloys, *Proceeding of the Institution of Mechanical Engineer Part B Journal of Engineering*
345 *Manufacturer*, 233, 2283–2291.
- 346 22. Sulaiman, K. O., Onawole, A. T., Faye, O., Shuaib, D. T. (2019). Understanding the corrosion
347 inhibition of mild steel by selected green compounds using chemical quantum-based
348 assessments and molecular dynamics simulations. *Journal of Molecular Liquids*, 279, 342–350.
349 <http://dx.doi.org/10.1016/j.molliq.2019.01.136>
- 350 23. Thakur, A., Kumar, A. (2023). Computational insights into the corrosion inhibition potential of
351 some pyridine derivatives: A DFT approach. *European Journal of Chemistry*, 14(2), 246-253.
352 <https://dx.doi.org/10.5155/eurjchem.14.2.246-253.2408>
- 353 24. Uzah, T. T., Mbonu, I. J. (2023). Insight into synergistic corrosion inhibition of thiourea and ZnCl₂
354 on mild steel: Experimental and theoretical Approaches. *Journal of Chemistry Letters*, 4, 211-
355 221. <https://doi:10.22034/jchemlett.2024.413932.1135>
- 356 25. Uzah, T. T., Mbonu, J. I. (2024). Enhancing the inhibition action of acetamide with iodide ions for
357 mild steel corrosion in 0.5 M H₂SO₄ environment. *Letters in Applied NanoBioScience*, 13, 1-16,
358 <https://doi.org/10.33263/LIANBS131.049>.
- 359 26. Uzah, T. T., Mbonu, J. I., Gber, T. E., Louis, H. (2023). Synergistic effect of KI and urea on the
360 corrosion protection of mild steel in 0.5 M H₂SO₄: Experimental and computational insights.
361 *Results in Chemistry*, 5, 1-9. <https://doi.org/10.1016/j.rechem.2023.100981>
- 362 27. Uzah, T.T. (2025) Theoretical evaluation of urea derivatives on Fe (110) and Sn (111) surfaces
363 in acidic medium: DFT and Monte Carlo simulation approaches. *Materials International*. 7(1), 1-
364 12 <https://doi.org/10.33263/Materials71.002>
- 365 28. Uzah, T. T. (2024). DFT and Monte Carlo simulation for the prediction of corrosion inhibitive
366 efficacy of selected thiosemicarbazide derivatives on Al (111) and Cu (111) Surfaces in Acidic
367 Media. *Journal of Medical and Nanomaterial Chemistry*, 6, 81-94,
368 <https://doi.org/10.48309/JMNC.2024.1.7>
- 369 29. Verma, C., Olasunkanmi, L. O., Ebenso, E. E., Quraishi, M. A., Obot, I. B. (2016). Adsorption
370 behavior of glucosamine-based, pyrimidine-fused heterocycles as green corrosion inhibitors for
371 mild steel: Experimental and Theoretical Studies. *The Journal of Physical Chemistry C*, 120,
372 11598-11611, <https://doi.org/10.1021/acs.jpcc.6b04429>.
- 373 30. Verma, D. K., Aslam, R., Aslam, J., Quraishi, M. A., Ebenso, E. E., Verma, C. (2021).
374 Computational modeling: theoretical predictive tools for designing of potential organic corrosion
375 inhibitors. *Journal of Molecular Structures*, 1236, 130294.
376 <https://doi.org/10.1016/j.molstruc.2021.130294>
- 377 31. Yang, W., Xu, D., Chen, J., Liu, J., Jiang, B. (2017). Characterization of self-sealing MAO
378 ceramic coatings with green or black color on an Al alloy. *RSC Advances*, 7, 1597-1605,
379 <https://doi.org/10.1039/C6RA25415B>.

